

# PINO - a tool for simulating neutron spectra resulting from the ${}^7\text{Li}(p,n)$ reaction

R. Reifarh<sup>a,b</sup>, M. Heil<sup>a</sup>, F. Käppeler<sup>c</sup>, R. Plag<sup>a,b</sup>

<sup>a</sup>*Gesellschaft für Schwerionenforschung mbH, Darmstadt, D-64291, Germany*

<sup>b</sup>*J.W. Goethe Universität, Frankfurt a.M, D-60438, Germany*

<sup>c</sup>*Forschungszentrum Karlsruhe, Postfach 3640, D-76021 Karlsruhe, Germany*

---

## Abstract

The  ${}^7\text{Li}(p,n)$  reaction in combination with a 3.7 MV Van de Graaff accelerator was routinely used at FZK to perform activation as well as time-of-flight measurements with neutrons in the keV-region. Planned new setups with much higher proton currents like SARAF and FRANZ and the availability of liquid-lithium target technology will trigger a renaissance of this method. A detailed understanding of the neutron spectrum is not only important during the planning phase of an experiment, but also during for the analysis of activation experiments. Therefore, the Monte-Carlo based program PINO (Protons In Neutrons Out) was developed, which allows the simulation of neutron spectra considering the geometry of the setup and the proton-energy distribution.

*Key words:* keV neutron source, Monte Carlo simulations

*PACS:* 29.25.Dz, 02.70.Uu

---

## 1 Introduction

The scope of this work was to provide a tool for experimentalists to estimate the neutron flux as a well as the neutron energy distribution during activation experiments using the  ${}^7\text{Li}(p,n)$  reaction as a neutron source. This method in combination with a Van de Graaff accelerator was used for almost thirty years at the Forschungszentrum Karlsruhe. A detailed description of the activation method for obtaining  $(n,\gamma)$  cross sections and the experimental setup can be found in literature [1, 2]. The essential features of such experiments

---

*Email address:* [r.reifarh@gsi.de](mailto:r.reifarh@gsi.de) (R. Reifarh).

consist of two steps, irradiation of a sample in a quasi-stellar neutron spectrum and the determination of the amount of freshly produced nuclei either via the induced activity [3] or via accelerator mass spectrometry (AMS) [4]. The development of new accelerator technologies, in particular the development of radiofrequency quadrupoles (RFQ) provides much higher proton currents than previously achievable. The additional development of liquid-lithium target technology to handle the target cooling opens a new era of activation experiments thanks to the enormously increased neutron flux. Projects like SARAF [5] and FRANZ [6], which are currently under construction underline this statement. Even though FRANZ allows also the preferable time-of-flight (TOF) method, the activation method, if applicable, remains the method of choice if the half-life of the isotope under investigation is too short or the sample mass too small. Many of the astrophysically interesting isotopes will have to wait for neutron sources even beyond SARAF or FRANZ, if a time-of-flight measurement is desired [7].

While other neutron-energy distributions were used on occasion [8, 9], the quasi-stellar neutron spectrum, which can be obtained by bombarding a thick metallic Li target with protons of 1912 keV, slightly above the reaction threshold at 1881 keV, was the working horse at the Forschungszentrum Karlsruhe [10]. Under such conditions, the  ${}^7\text{Li}(p,n){}^7\text{Be}$  reaction yields a continuous energy distribution with a high-energy cutoff at  $E_n = 106$  keV. The produced neutrons are emitted in a forward cone of  $120^\circ$  opening angle. The angle-integrated spectrum closely resembles a spectrum necessary to measure the Maxwellian averaged cross section at  $kT = 25$  keV:

$$\frac{dN}{dE} = E \cdot e^{-\frac{E}{kT}} = \sqrt{E} \cdot \Phi_{Maxwell}, \quad (1)$$

where  $\Phi_{Maxwell}$  is the Maxwellian distribution for a thermal energy of  $kT = 25$  keV [11].

The samples are typically sandwiched between gold foils and placed directly on the backing of the lithium target. A typical setup is sketched in Fig. 1. The simultaneous activation of the gold foils provides a convenient tool for measuring the neutron flux, since both the stellar neutron capture cross section of  ${}^{197}\text{Au}$  [11] and the parameters of the  ${}^{198}\text{Au}$  decay [12] are accurately known.

While the neutron spectrum for the standard case is very well understood, a tool for extrapolation to different experimental conditions is desired. Such changes of the standard setup typically include differences in the angle coverage of the sample, a different thickness of the lithium layer, or different proton energies. The extrapolation is, while conceptually obvious, not straight forward. After impinging onto the lithium layer, the protons are slowed down until they either leave the lithium layer (in case of a very thin layer) or are be-

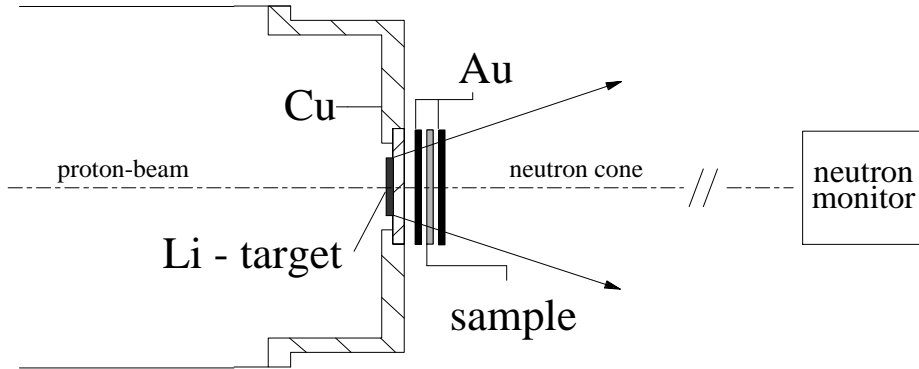


Fig. 1. Typical activation setup at the Forschungszentrum Karlsruhe. Neutrons are produced via the  ${}^7\text{Li}(p,n)$  reaction just above the production threshold. The emitted neutrons are then kinematically focussed into a cone with an opening angle of  $120^\circ$ . The sample is usually sandwiched by two gold foils in order to determine the neutron flux just before and behind the sample.

low the (p,n) reaction threshold and do not contribute to the neutron production anymore. The double-differential (p,n) cross section changes significantly during this process, especially in the energy regime close to the production threshold. Additionally the kinematics of the reaction is important during the process. Since the Q-value of the reaction is positive, the reaction products, and the neutrons in particular, are emitted into a cone in the direction of the protons (Fig. 1). This effect becomes less and less pronounced as the proton energy increases. If the proton energy in the center-of-mass system is above 2.37 MeV, a second reaction channel  ${}^7\text{Li}(p,n){}^7\text{Be}^*$  opens, which leads to a second neutron group at lower energies.

To model these processes quantitatively, a tool to simulate the neutron spectrum resulting from the  ${}^7\text{Li}(p,n)$  reaction with a Monte-Carlo approach is indispensable. Therefore we developed the highly specialized program PINO - Protons In Neutrons Out.

## 2 PINO - the program

### 2.1 General approach

The Monte-Carlo approach means that for each neutron, at first a randomly chosen energy will be assigned to a proton. This happens according to the energy distribution of the proton beam. Then the proton energy at the event of an interaction in the lithium layer will be randomly determined. If  $E_p$  is the proton energy and  $z$  the depth inside the lithium layer, the stopping power is

defined as:

$$S = -\frac{dE_p}{dz} \quad (2)$$

The the proton energy as a function of position inside the lithium layer can then be written as:

$$E_p(z) = E_p(0) - \int_0^z S(E_p(z'))dz' \quad (3)$$

or the depth as a function of energy using the projected range  $z(E_p, E_p(0)) = R(E_p(0)) - R(E_p)$ . For the interaction probability as a function of depth one finds  $dP/dE(z) \propto \sigma_{(p,n)}(E_p(z))$ , or as a function of energy:

$$\frac{dP}{dE}(E) \propto \frac{\sigma_{(p,n)}(E)}{S(E)}. \quad (4)$$

Hence the total interaction probability is:

$$P_{total}(E_p) \propto \int_{E_{threshold}}^{E_p} \frac{\sigma_{(p,n)}(E)}{S(E)}dE. \quad (5)$$

After the determination of the interaction energy, the emission angle and energy are randomly acquired based on the double-differential  ${}^7\text{Li}(p,n)$  cross section fulfilling momentum and energy conservation laws. Finally the neutron will be tracked through the imaginary sample.

## 2.2 Proton transport

Protons are not fully tracked. The simplified assumption was made that the protons do not scatter in the thin lithium layer. The only interactions considered are the ionization of lithium, hence the stopping of the protons because of electronic interactions, and (p,n) reactions. The stopping power data (see equation (2) ) are read in from a separate file, which can be initialized at the beginning of the program (see Sect. 2.5). All results shown in this paper are based on stopping power data from the well-established program SRIM [13].

### 2.3 The (p,n) reaction

Under the conditions typically simulated here, the total interaction probability is in the order of  $10^{-6}$ . In order to simplify the calculations it is therefore assumed that the total interaction probability is much smaller than one. In other words, the self-shielding of the lithium layer is neglected. The advantage of this assumption is, that the (p,n) cross section can then be scaled such that for each proton exactly one neutron is produced in the simulation. This scaling factor is the total neutron production yield  $P_{total}$ , see equation (5). The interaction probability used in the code is then:

$$\frac{dP_{code}}{dE}(E) = \frac{1}{P_{total}} \frac{\sigma_{(p,n)}(E)}{S(E)}, \quad (6)$$

hence  $P_{code,total}(E_p) = 1$ .

The cross section data are read in from a separate file, which can be initialized at the beginning of the program (see Sect. 2.5). All results shown in this paper are based on the double-differential cross sections compiled by Liskien and Paulsen [14].

### 2.4 Neutron transport

Similarly to the protons, also the neutron transport is very simplified. In the typical applications considered here, the backing of the lithium layer as well as the sample were thin enough to result in transmission coefficients above 95%. The neutrons are therefore not tracked, but rather ray-traced. Only position and angle at the time of production are considered.

### 2.5 Input and Output

Each simulation requires an input file, which contains information about the geometry as well as cross sections and output options. The first three lines of the input file refer to the files containing the double-differential  ${}^7\text{Li}(p,n){}^7\text{Be}$  and  ${}^7\text{Li}(p,n){}^7\text{Be}^*$  cross sections and the stopping power data. Modification of these input parameters allows for instance the simulation of chemical compounds of lithium, like the thermally very robust compositions LiF or Li<sub>2</sub>O.

The next lines define the proton energy and energy spread, thickness of the lithium layer, and the number of samples. Finally, the last lines are defining the geometry for the emitted neutrons and contain information about the size of

the lithium spot hit by the proton beam, the distance from sample to lithium layer, and the geometry of the sample (shape, dimensions). For convenience, an optional line allows a reference to a neutron capture cross section file and the resulting neutron spectrum will be folded with this cross section.

At the end of each simulation two output files are generated. One contains neutron yields as a function of energy. Only neutrons passing the sample are considered and output is generated for  ${}^7\text{Li}(p,n){}^7\text{Be}$  and  ${}^7\text{Li}(p,n){}^7\text{Be}^*$  separately. Additionally, both outputs are given with an angular weighting. If neutrons pass a disk not perpendicular to the surface, the effective sample thickness changes by a factor  $\cos(\vartheta)$ . The other file contains a suite of useful information for the planning and analysis of an experiment. Amongst them are the number of neutrons passing the sample, the number of neutrons per proton current, the effective lithium thickness, the particular layer after which protons are below the neutron production threshold, and the neutron capture cross section folded with the neutron spectrum derived for the sample.

## *2.6 Limitations and possibilities*

As already discussed in Secs. 2.2 through 2.4 the particle transport is simplified. In particular straggling of the protons in the lithium layer is not considered. This is a valid assumption for the typical applications described in Sec. 3, where the range of the protons above the neutron production threshold is very small. If however, one would choose significantly higher proton energies and respectively thicker lithium layers, the proton straggling will lead to a more isotropic neutron emission than predicted by the program, since the protons might change direction before interacting with the  ${}^7\text{Li}$  nucleus.

Similarly the simplified neutron transport is only valid for the cases described before. If the interaction probability in the sample or backing can not be neglected anymore, because of thicker backings or samples, the simulation may result in significant differences from reality.

If however, the described simplifying assumptions are valid, the program is very flexible, easy to use, and very fast. A typical simulation with  $10^9$  protons on a standard Laptop (Intel processor, 2 GHz) takes only minutes, which means that situations with  $10^9$  neutrons can be simulated. Depending on the problem however,  $10^7$  emitted neutrons are often already sufficient, resulting in simulation times of a few seconds. PINO will therefore be made available as a web-application at the URL: <http://exp-astro.physik.uni-frankfurt.de/pino>

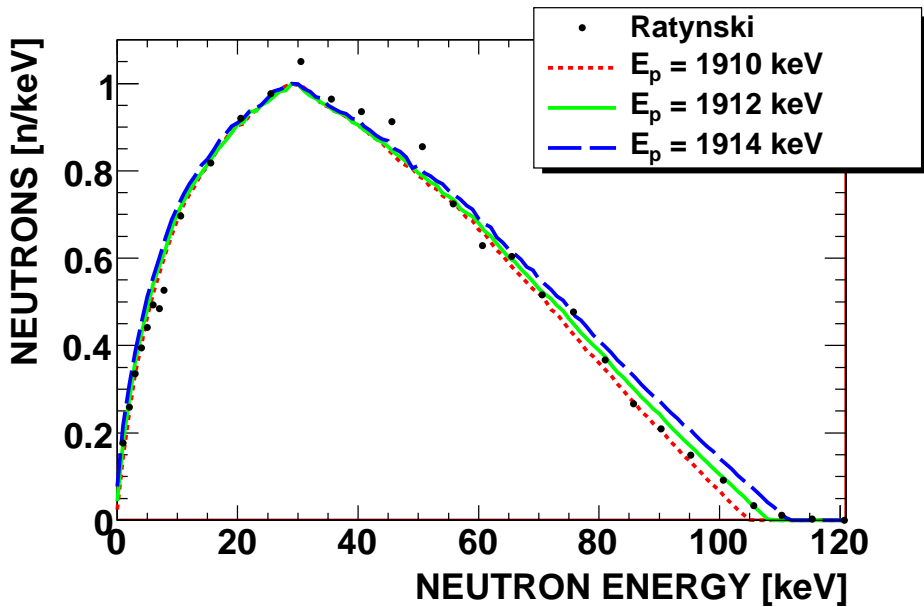


Fig. 2. Comparison of the number of angle-integrated neutrons per linear energy bin for measured data [11] with simulation results that contain no weighting with the angle-dependent sample thickness. All simulated spectra are normalized to a common maximum of 1.

### 3 PINO - results

#### 3.1 Comparison with measured data

A first test of the performance was the comparison with the experimentally determined neutron spectrum at the Forschungszentrum Karlsruhe by Ratynski and Käppeler [11]. We feel, it is important to point out that the spectrum measured and published there is not the spectrum seen by a disk-like sample. In the spectrum measurement, the same neutron detector was positioned at different angles with respect to the proton-beam axis. The surface of this detector was always perpendicular to the direction of the emitted neutrons. Therefore, the effective thickness of the detector was constant for all neutron emission angles. In contrast, the effective thickness of a disk-like sample changes as a function of emission angle (see also Sec. 2.5).

Fig. 2 shows the comparison of the experimental data with simulations of different incident proton energies. The data agree very well for the nominal proton energy of 1912 keV as well as for energies slightly above or below. This gives additional confidence in the experimental method, since the proton energy might fluctuate slightly during the sometimes extended neutron activation experiments.

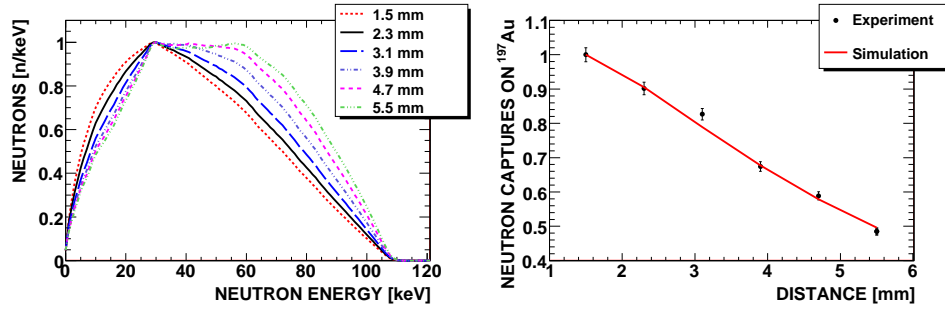


Fig. 3. Left: Simulated neutron spectra for the stack of gold foils with 5 mm diameter (see also Fig. 2). Right: Comparison of experimental data with simulation results. The data are normalized to the point at 1.5 mm.

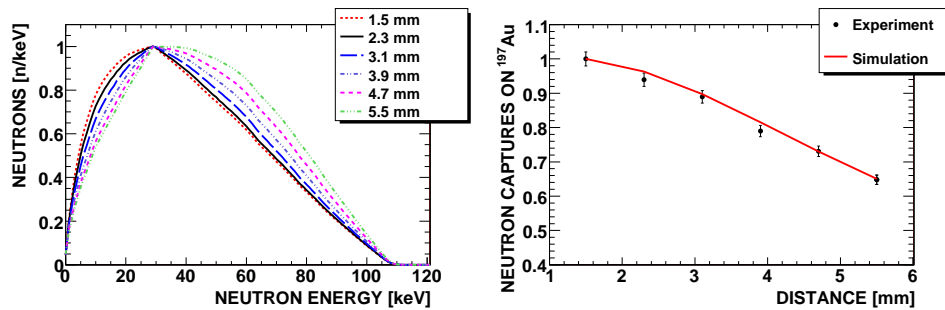


Fig. 4. Left: Simulated neutron spectra for the stack of gold foils with 10 mm diameter (see also Fig. 2). Right: Comparison of experimental data with simulation results. The data are normalized to the point at 1.5 mm.

A second test was the comparison with an activation of a stack of gold foils [15]. It was found that over a range of 6 mm, the induced activity in a stack of gold foils depends linearly from on the distance between the gold foils and the lithium spot. This simple behavior was found for gold foils of 5 and 10 mm in diameter. While the behaviour is simple, it is not so simple to explain, since the solid angle coverage changes non-linearly and additionally the averaged  $^{197}\text{Au}(n,\gamma)$  cross section changes because the different foils are exposed to different neutron spectra. It is therefore an interesting test for the simulation tool described here. Figs. 3 and 4 show the simulated neutron spectra and a comparison between experimental and simulated number of neutron captures on  $^{197}\text{Au}$  for the two foil diameters. The agreement even in these two cases is so good that we felt comfortable using this simulation tool for a number of other applications without further verification.

### 3.2 Other simulation results

In this section a few applications of the simulation tool will be presented, which have not been discussed so far in this paper or in previous publications.



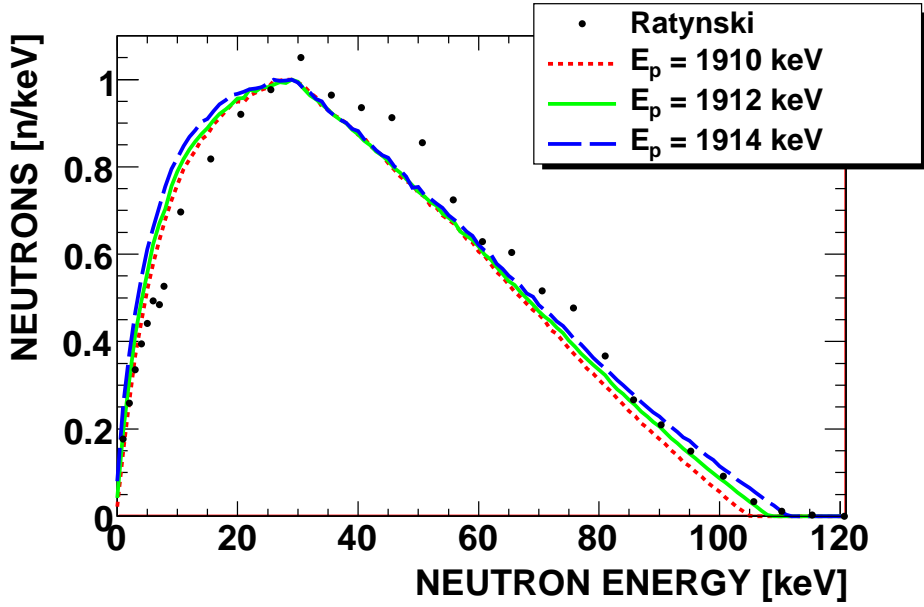


Fig. 5. Comparison of the number of angle-integrated neutrons per linear energy bin for experimental results and simulations including weighting with the angle-dependent sample thickness. All simulated spectra are normalized to a common maximum of 1.

A natural first application was to simulate the actual neutron spectrum of the "standard" setup at the Forschungszentrum Karlsruhe. Standard setup in this case means that the sample dimensions are such that the entire neutron cone is covered by a disk-like sample. Fig. 5 shows the result of such a simulation. Obviously the simulated spectrum is slightly shifted towards lower energies compared to the Ratynski et al. spectrum [11] (to be compared to Fig. 2). The reason is that low-energy neutrons are preferably emitted at high emission angles and they get more weight for a disk-like sample.

An interesting question is what happens, if only a part of the neutron cone is covered, because the sample is too small. The question is addressed in Fig. 6. The simple picture, that with smaller angular coverage the neutron spectra are approaching the Ratynski et al. spectrum again, holds true.

While the energy uncertainty at Van de Graaff accelerators is in the order of 0.1%, RFQ based accelerators have typically uncertainties in the order of 1%. In view of the upcoming FRANZ facility, where an energy uncertainty around 20 keV is expected, a simulation with the corresponding parameters has been performed. Fig. 7 shows the result of such a simulation in comparison with the much sharper situation at a Van de Graaff accelerator and the ideal Maxwellian averaged spectrum corresponding to  $kT = 24$  keV. The sharp drop of the Van de Graaff spectrum at the maximum neutron energy around 110 keV is significantly smeared out. This means that one of the disadvantages

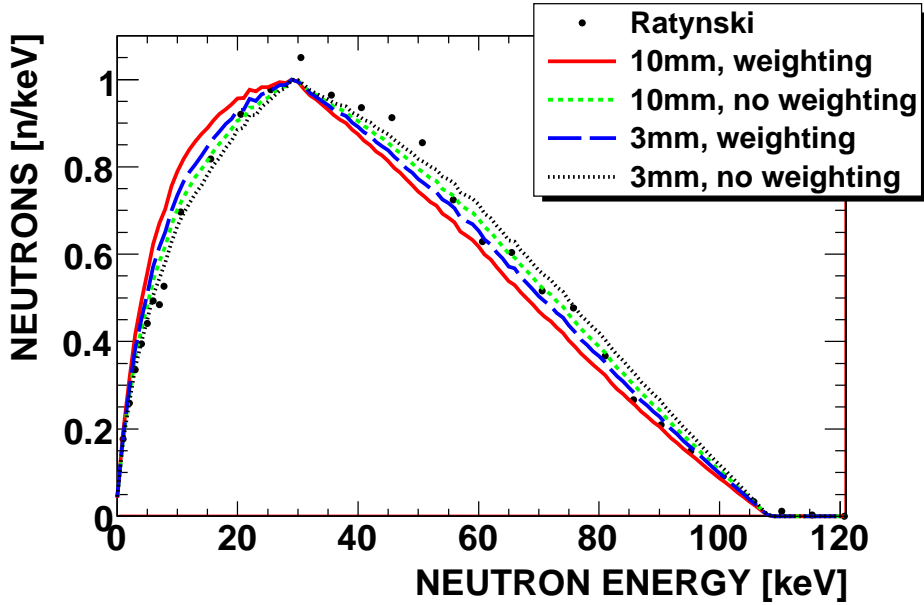


Fig. 6. Comparison of the number of angle-integrated neutrons per linear energy bin for simulations that contain weighting and no weighting for a sample covering the entire neutron cone (10 mm radius) and only part of the cone (3 mm radius). The radius of the Li-spot was 3 mm. All simulated spectra are normalized to a common maximum of 1.

of the activation method as applied at the Forschungszentrum Karlsruhe is actually almost entirely removed. A hypothetical, strong resonance at 120 keV would have been overlooked with the sharp edge, but would contribute at least to a certain extent at the broadened spectrum.

#### 4 Summary

Driven by the needs of planning and analyzing neutron activation experiments at the Forschungszentrum Karlsruhe, we developed a flexible tool to simulate the produced neutron spectra. Within the simplifying assumptions concerning proton and neutron transport the program described here is well suited for the parameter space of typical activation experiments using thin lithium layers and the  ${}^7\text{Li}(p,n)$  reaction. However, the code is of very restricted applicability outside of this parameter space.

We compared the resulting simulated neutron spectra with available experimental data and found very good agreement. The program was already used undocumented during the analysis of a number of experiments and will also be useful for determining neutron spectra and for estimating neutron exposures at upcoming other facilities.

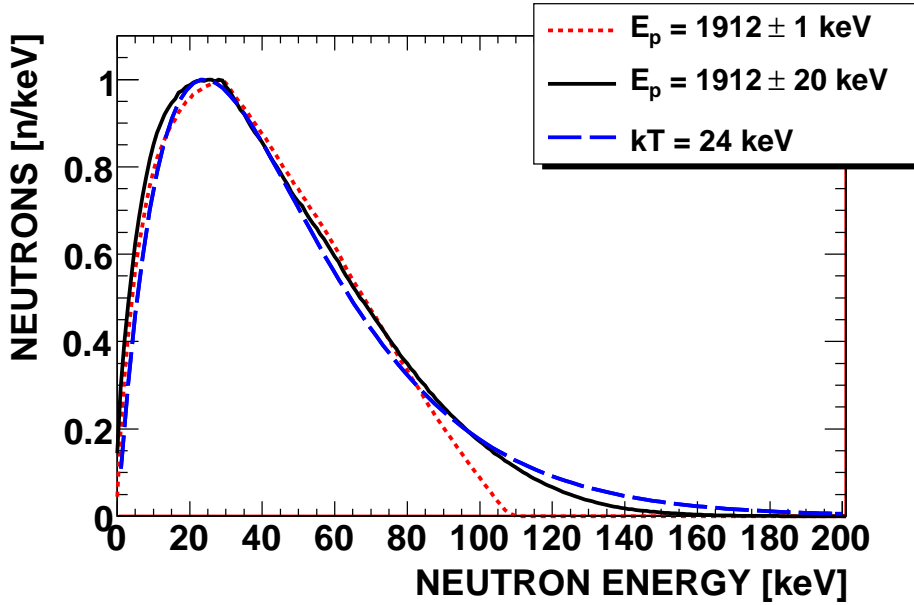


Fig. 7. Comparison of the number of angle-integrated neutrons per linear energy bin for simulations that contain weighting and include a gaussian proton energy profile. A sample of 10 mm radius and a Li-spot of 3 mm radius was assumed. All simulated spectra are normalized to a common maximum of 1.

PINO will be made available as a web-application at the URL: <http://exp-astro.physik.uni-frankfurt.de/>

### *Acknowledgments*

R.R. and R.P. are supported by the HGF Young Investigators Project VH-NG-327. We thank A. Plompen for his helpful comments on the manuscript.

### **References**

- [1] H. Beer, F. Käppeler, Phys. Rev. C 21 (1980) 534 – 544.
- [2] K. Toukan, K. Debus, F. Käppeler, G. Reffo, Phys. Rev. C 51 (1995) 1540 – 1550.
- [3] R. Reifarh, F. Käppeler, Phys. Rev. C (Nuclear Physics) 66 (5) (2002) 054605.
- [4] H. Nassar, M. Paul, I. Ahmad, D. Berkovits, M. Bettan, P. Collon, S. Dababneh, S. Ghelberg, J. P. Greene, A. Heger, M. Heil, D. J. Henderson, C. L. Jiang, F. Käppeler, H. Koivisto, S. O’Brien, R. C. Pardo, N. Patronis, T. Pennington, R. Plag, K. E. Rehm, R. Reifarh, R. Scott, S. Sinha, X. Tang, R. Vondrasek, Phys. Rev. Let. 94 (2005) 092504.
- [5] A. Nagler, I. Mardor, D. Berkovits, C. Piel, P. vom Stein, H. Vogel, Sta-

- tus of the saraf project, in: LINAC 2006, Joint Accelerator Conferences Website, Knoxville, TN, 2006, p. MOP054.
- [6] O. Meusel, L. P. Chau, I. Mueller, U. Ratzinger, A. Schempp, K. Volk, C. Zhang, Development of an intense neutron source franz in frankfurt, in: LINAC 2006, Joint Accelerator Conferences Website, Knoxville, TN, 2006, p. MOP051.
  - [7] A. Couture, R. Reifarh, Atomic Data and Nuclear Data Tables 93 (2007) 807.
  - [8] R. Reifarh, K. Schwarz, F. Käppeler, Ap. J. 528 (2000) 573 – 581.
  - [9] R. Reifarh, M. Heil, C. Forssén, U. Besserer, A. Couture, S. Dababneh, L. Dörr, J. Görres, R. C. Haight, F. Käppeler, A. Mengoni, S. O'Brien, N. Patronis, R. Plag, R. S. Rundberg, M. Wiescher, J. B. Wilhelmy, Phys. Rev. C 77 (2008) 015804.
  - [10] Z. Y. Bao, H. Beer, F. Käppeler, F. Voss, K. Wisshak, T. Rauscher, Atomic Data Nucl. Data Tables 76 (2000) 70.
  - [11] W. Ratynski, F. Käppeler, Phys. Rev. C 37 (1988) 595 – 604.
  - [12] R. Auble, Nucl. Data Sheets 40 (1983) 301.
  - [13] J. Ziegler, Handbook of Stopping Cross-Sections for Energetic Ions in all Elements, Vol. 5, Pergamon Press, New York, 1980, this is a full BOOK entry.
  - [14] H. Liskien, A. Paulsen, Atomic Data and Nucl. Data Tables 15 (1975) 57.
  - [15] R. Reifarh, C. Arlandini, M. Heil, F. Käppeler, P. Sedychev, A. Mengoni, M. Herman, T. Rauscher, R. Gallino, C. Travaglio, Ap. J. 582 (2003) 1251.